Oil-in-water droplets generation in dripping regime with channel partial wetting

Nathalie Tarchichi   Franck Chollet*
Jean-François Manceau
FEMTO-ST Institute, Université de Franche-Comté
15B avenue des Montboucons, 25030 Besançon cedex, France

February 28, 2016

Abstract

We generated silicone oil micro-droplet in deionized water with a microfluidic T-junction devices made on silicon-glass with different cross-sections (depth and width) of the continuous phase and the dispersed phase micro-channels. We experimentally show that the size of the droplet decreases when the width or the velocity of the dispersed phase micro-channel decreases but is almost insensitive to the channel depth. For describing the observed behaviour, we proposed a modified mechanism of droplet formation consisting of three stages, each with start and end precisely identified. Based on this mechanism, we developed an analytical model for obtaining the droplet diameter in dripping regime when there is partial wetting at the channel boundary. This model is in better agreement with the experiments than other analytical models from the literature, suggesting the effect of channel wetting is significant. We also discuss the use of the capillary number in models, and suggests that the velocity would be a better metrics for comparing different T-junction geometry. In the experiment, the generated droplet diameter is varied between 28 µm and 196 µm.

1 Introduction

Microfluidic devices have been developed since a decade for different applications in various industries: foods, pharmaceuticals, cosmetics, electronics, etc [1]. Among these applications of microfluidic systems, many of them are based on the dispersion of a fluid in another immiscible fluid. These two-phase flow systems appear in different fields such as medical science [2], chemistry, sensing [3], etc. For many of these applications, it is crucial to generate uniform droplets (liquid-liquid system) or bubbles (liquid-gas system), and control their size.

In recent years, different structures have been proposed to produce monodisperse droplets or bubbles. The most widely used are the T-junction [4], the flow-focusing [5], and the co-flowing devices [6].
Several authors have also studied the parameters controlling the droplet or bubble size and their generation mode. These parameters include the channel geometry, the flow rates, the interfacial or the surface tension, the viscosity of the fluids, etc [7, 8].

In the T-junction device the continuous phase and the dispersed (immiscible) phase are introduced into a main channel and a cross-channel, respectively. The break-up of the fluid in droplets or bubbles is mostly triggered by the flow induced pressure gradient and drag force appearing at the junction.
In this configuration, there are three main identified regimes of droplets or bubbles generation (squeezing, dripping and jetting) and an additional balloon regime that we recently put in evidence at very low dispersed phase velocity[9]. Many authors have been interested in the study of the squeezing and the dripping regimes, as well as the study of the transition between these two modes of generation, producing multiple experimental and theoretical studies for modeling the laws governing the droplet size.

In the squeezing regime, Garstecki [10] proposed, after a detailed analysis of the different physical forces present in the system, a simple equation binding the droplet length L to the two fluids flow rates ratio:

$$L = w_c(1 + \alpha \frac{Q_d}{Q_c})$$ (1)

where α is a geometrical factor close to 1, and Q_d, Q_c are the dispersed and continuous fluids flow rates, respectively. This linear equation was obtained by considering that the droplet generation process occurs in two steps. First, the dispersed phase enters and fills the continuous phase micro-channel, resulting in a droplet whose length is

*Address correspondence to this author at the FEMTO-ST Institute, Université de Franche-Comté, 15B avenue des Montboucons, 25030 Besançon cedex, France; Tel: +33 363082458; Email: franck.chollet@femto-st.fr

equal to the width of the continuous phase micro-channel w_c. Then, the droplet starts moving away from the dispersed phase channel while growing before it finally detaches. Actually, blocked by the droplet, the pressure increases upstream in the continuous phase micro-channel, squeezing the neck of the dispersed phase droplet. The time t_{neck} necessary to fully detach the droplet is empirically related to the continuous phase velocity ($v_c = \frac{Q_c}{hw_c}$, with Q_c the flow rate of the continuous phase, h the micro-channel depth and w_c the width of the continuous phase micro-channel) by $t_{neck} = \frac{d}{v_c}$ where d is the width of the neck. During this time, the droplet grows at the dispersed phase rate $v_{growth} = v_d = \frac{Q_d}{hw_d}$, with Q_d the flow rate of the dispersed phase, h the micro-channel depth and w_d the width of the dispersed phase micro-channel. So the final length of the droplet is: $L = w_c + t_{neck}\frac{Q_d}{hw_d}$, giving equation 1.

Several authors have used this linear equation by adapting it to their experimental observation for non-square channel section. Thus, Xu et al. [11] found that $L = w_c(1.38 + 2.52\frac{Q_d}{Q_c})$, while Fu et al. [12] wrote $L = w_c(0.64 + 0.32\frac{Q_d}{Q_c})$, etc.

In the dripping regime, some authors have modeled the droplet size based on a force balance between the interfacial force and the viscous force at the junction. Actually the modeling of the droplet formation mechanism in the dripping regime was initiated by Thorsen in his seminal paper[4], where, basing his analysis on analogies with the formation of emulsion described by Taylor et al. [13], he found a simple equation for estimating the droplet diameter as a function of the capillary number of the continuous phase ($Ca_c = \frac{\mu_c v_c}{\sigma}$, with μ_c the continuous phase viscosity, v_c the continuous phase velocity and σ the interfacial tension):

$$\frac{d}{w_c} \approx \frac{1}{Ca_c} \qquad (2)$$

where d is the droplet diameter, and w_c is the width of the continuous phase micro-channel. Nisisako et al. [14] and Cristini and Tan [15] have obtained similar results. Xu et al. [11] found that the model using by Thorsen [4] is compatible with their experimental results only for a $Ca_c > 0.2$. For $Ca_c < 0.2$, they proposed a modification of equation 2, and they wrote: $\frac{d}{w_c} \approx \frac{1}{Ca_c} \cdot \frac{w_c h - 0.785 d^2}{w_c h}$, where h is the micro-channel height. While, Fu et al. [12] expressed the diameter of the droplet as follows: $\frac{d}{w_c} = 1.42 Ca_c^{-0.11}$, etc.

Another way of expressing the droplet size, in the dripping regime, without using the dimensionless number Ca is to identify different stages of droplet formation, as in the case of the squeezing regime. Thus, Van der Graaf et al. [16] proposed that the droplet growth mechanism is split in two phases: a first phase of growth lasting until the drag force on the droplet equals the retaining interfacial tension force appearing at the dispersed phase channel

mound (V_{crit}), and a second inflating phase lasting t_{neck}, the time it takes for the continuous phase to squeeze the neck of the droplet and to free it completely. The duration of this second phase is not given explicitly and to find the volume of the droplet V_f he wrote, $V_f = V_{crit} + t_{neck}Q_d$, where Q_d is the flow rate of the dispersed phase. This idea of a two-phase formation process is actually inspired by a paper of Peng et al. [17], where droplet formation on a membrane, thus free from channel walls interaction, is described similarly, with V_{crit} given as a force or a torque equilibrium between surface tension at the mound of the dispersed phase pore and the sum of the drag and buoyancy effects.

Christopher [18] adapted the work of Garstecki [10] to the dripping regime by writing, as Taylor [13] before, an equilibrium of forces to obtain V_{crit}, taking for the retaining force the Laplace pressure [10] and for the drag force the sum of a shear component [4] and a pressure force estimated by the pressure drop along the length of the droplet in the main channel. This model describes for the first time the retaining force as the Laplace pressure difference arising because of the difference in radius of curvature at the upstream and the downstream ends of the droplet ($F_\sigma = -\sigma h$) instead of the interfacial tension force at the mound of the dispersed phase channel [17, 16]. For the second phase the time for squeezing the neck is again empirically estimated by assuming that $t_{neck} \approx \frac{w_d}{v_c}$, where w_d is the width of the dispersed phase channel and v_c the velocity of the fluid in the continuous phase channel.

As Yeom et al.[19] have shown, there are still many cases where none of the previous models seem to describe fully the experimental condition and they choose to fit the model to a set of experimental data. In their work, they considered that the mechanism of droplets formation is composed of two stages, without precisely specifying the boundary between these two stages, and used five parameters to fit V_{crit} and five other parameters to fit t_{neck}. If their model fits well the tested experimental data, the large number of fitted parameters seems to loose the direct link between the model and the experiment, and pinpoints that the analytical models used probably need further refining for representing better the physical phenomena at play.

The transition between the dripping and the squeezing regimes is described by several authors[10, 20, 11, 12, 21] using the capillary number of the continuous phase Ca_c. These works find a critical value that separates these two droplet generation regimes. Garstecki [10] and Menech [20] place the critical value at $Ca_{c(critical)} \approx 10^{-2}$. When $Ca_c < 10^{-2}$, the interfacial tension dominates the shear force linked to the presence of the continuous phase stream, and the detachment is caused by the pressure drop across the plug, while when $Ca_c > 10^{-2}$, the shear force controls the droplet detachment and the dripping

regime is present. If the general argument is certainly relevant, newer experiments tend to show that the exact value of $Ca_{c(critical)}$ is probably not significant since different authors find different values from their experimental or numerical observations. To name just a few literature references, we note that Xu et al. [11] found that the dripping regime is obtained for $0.01 < Ca_c < 0.3$, and the squeezing regime is observed for $Ca_c < 0.002$, Fu et al. [12] showed that the dripping regime and the squeezing regime are present for $0.013 < Ca_c < 1$, and $10^{-4} < Ca_c < 0.0058$ respectively, while Sivasamy et al. [21] observed the dripping regime for $Ca_c = 0.025$ and the squeezing regime for $Ca_c = 0.01$. The variation in this parameter indicates probably that different microfluidic systems have different behavior in this aspect that can not be grasped by a single number.

In the present work, we choose to study oil-in-water micro-droplets using a T-junction microfluidic device in the same silicon device used in our previous work [22] to see the effect of partial wetting on the dripping regime. Moreover, it seems that since the earlier work [4] most of the experiment have been conducted in polymer system [23, 24], favoring water-in-oil droplets. The silicon is thus chosen for its hydrophilicity (when it is covered by native oxide) and also for its toughness yielding more repeatable experiments.

We will show that with this technology the dripping regime is obtained at a very low value of continuous phase capillary number and that the droplet size varies with the width of the dispersed channel and the velocity of the dispersed phase. Taking into account the specificity of our setup, we propose a modified model, composed of three stages for describing the mechanism of droplet formation that could explain this behavior. The model precisely defines the beginning and the end of each stages and a comparison with existing models indicates some unique behavior in our setup.

2 Experiments

All microfluidic devices were prepared in the clean room of the FEMTO-ST Institute using silicon and Pyrex glass wafers with 500 µm thickness, and used a T-junction configuration. Figure 1 shows the steps used in the fabrication of the microfluidic devices. First we etched in the silicon wafer micro-channels of different depths (23, 46, 72 µm) by deep reactive ion etching (DRIE). At this step, an Alpha-step surface profiler is used to measure the micro-channel depth. Then a second DRIE step on the backside of the silicon wafer is realized in order to etch the through holes used for fluid injection. The channels are then sealed with a glass wafer using anodic bonding, providing a closed and transparent system before 22G flat-tip needles are glued to the fluid ports.
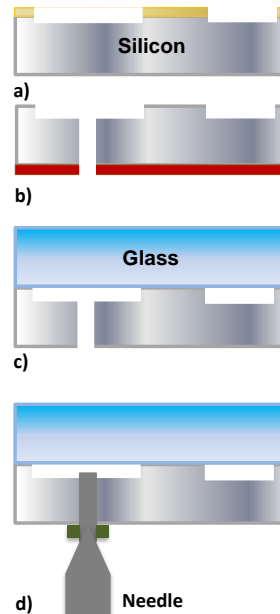

Figure 1: Fabrication process of microfluidic device: front-side photolithography using SPR220 photoresist (2.2µm) and micro-channels etching (a), back-side photolithography using thick AZ9260 photoresist (7µm) and through-holes etching (b), anodic bonding with pyrex glass (c), needle gluing with dual-part adhesive (d).

For the experiments in the dripping regime, we studied the effect of the cross-section geometry on the droplet size variation when the continuous phase velocity is varied.
For studying the effect of the cross-section of the dispersed phase micro-channel, we fixed the width of the continuous phase micro-channel ($w_c = 100$ µm) and we changed the width of the dispersed phase micro-channel ($w_d = 10$, 20 and 50 µm) (Figure 2). Actually, the dispersed phase micro-channels have a nominal width of 100 µm to reduce the overall pressure drop in the device and becomes narrower only 500 µm from the junction.
Similarly, for studying the effect of the cross-section of the continuous phase micro-channel, we fixed the width of the dispersed phase micro-channel ($w_d = 20$ µm) and we changed the width of the continuous phase micro-channel from one device to another ($w_c = 50$, 100 and 200 µm).

For generating oil droplets, silicone oil (Dow Corning 704® with dynamic viscosity of 39 mPa·s (density of 1070 kg/m³), and deionized water (viscosity 1 mPa·s) are used as the dispersed and the continuous phases, respectively. The aqueous solution was colored with a blue food dye to achieve better optical contrast. The interfacial tension oil-water was 100 mN/m without surfactant as measured with a Krüss tensiometer. This rather high value can be explained by the high chemical purity of both oil and water used that were not contaminated
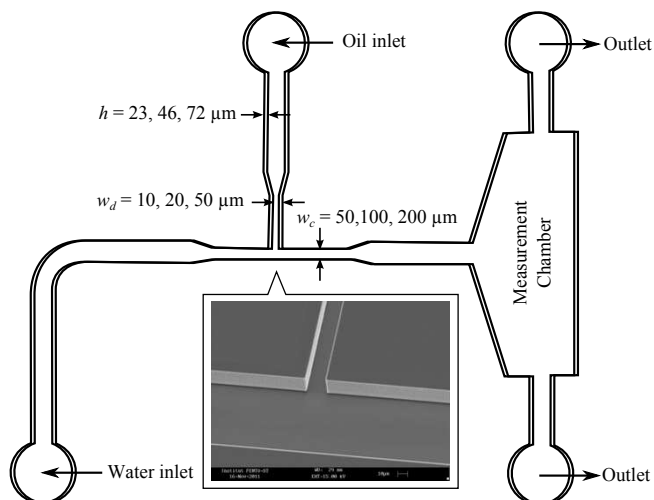
Figure 2: Schematic of the microfluidic system used in the generation of micro-droplets. (inset) SEM view of the etched T-junction with $w_c = 100$µm, $w_d = 10$µm and $h = 23$µm.

in the glass-silicon system [25]. Experiments were conducted at constant temperature $(20 \pm 2°C)$ using two syringe pumps to control the flow rates of the aqueous and oil phases in the micro-channels. The oil velocity $\overline{v_d}$ varied between 0.75 and $3\,\mathrm{cm/s}$ while the water velocity $\overline{v_c}$ was varied between 0.1 and $60\,\mathrm{cm/s}$ (corresponding to $10^{-5} < Ca_c < 6.10^{-3}$). After any change of the aqueous phase velocity we waited until we obtained stabilized droplet generation. The droplets diameter was then measured using a microscope and a CCD camera with a high speed shutter in a chamber located downstream a few millimeters after the T-junction. The polydispersity in the generated droplet was eventually measured below 2% in accordance with literature results on similar systems[4].

In the present work we have observed that the dripping regime is obtained at very low continuous phase capillary number: $2.10^{-4} < Ca_c < 6.10^{-3}$ and the squeezing regime at even smaller continuous phase capillary number $Ca_c < 5.10^{-5}$. Actually the use of water as continuous phase (a liquid with low viscosity) and, less importantly, the use of a special oil providing a high interfacial tension (100 mN/m) as dispersed phase, explain this low values of Ca_c. Still, these observations when compared to the literature tend to confirm that the value of the continuous phase capillary number Ca_c is not a magic number and becomes physically meaningful only when we compare the different regimes of droplet generation in the same microfluidic system. It therefore amounts mostly to compare the velocity of the continuous phase $\overline{v_c}$. Additionally, we note that in our previous work [9], we showed that the continuous phase capillary number alone can not predict the droplet generation mode but also requires the dispersed

phase capillary number Ca_d – and particularly the dispersed phase velocity $\overline{v_d}$. Actually, by controlling $\overline{v_d}$, we have demonstrated that it is possible to switch from dripping regime to a new regime of droplet generation that we called the balloon regime [9], whose behavior may be attributed to some partial wetting of the channel floor and ceiling. Another possible choice of flow variable in the literature is the flow rate $Q = \overline{v}A$. However it depends on the cross-section A of the microfluidic channels and as the cross-section varies in this work, the velocity is again a better variable as it allows direct comparison between different T-junction geometries.

We verified that a good repeatability could be obtained over a sufficiently long period. Actually we used the same chip and measured the variation of the droplet diameter as a function of the continuous phase velocity over 90 days (Figure 2). The chip could be used over 70 days with very repeatable results (less than 5% error, close to the limit of repeatability of the syringe pump and the measurement system), but failed to generate droplets at 90 days presumably because contamination modified the wetting properties at the T-junction. The transition was brutal and no progressive aging was observed in the evolution of the droplet diameter over time, presumably because its effect was smaller than the accuracy of the flow control.
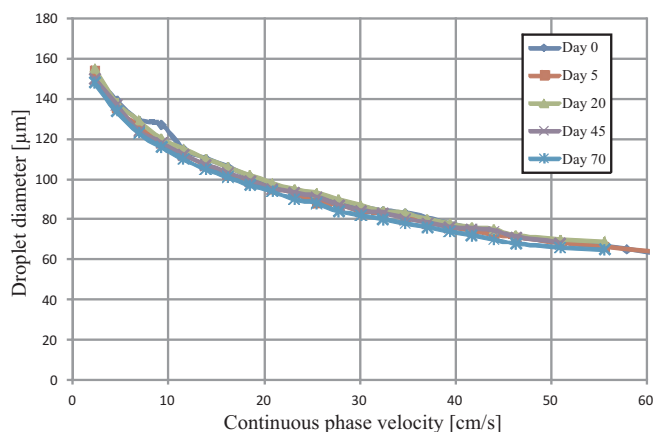

Figure 3: Variation of droplet diameter as a function of continuous phase velocity measured for 70 days ($h = 72$µm, $w_c = 100$µm, $w_d = 50$µm). Droplet generation did not work anymore after 90 days.

The 3D shape of the droplet is a matter of some controversy when only observation with a microscope can be performed. Actually we perform microscopic observation from the top and observe a circular droplet, but the profile along the depth is unknown. When the diameter d of the drop is larger than the depth of the channel h, we have the case shown in Figure 4-a, and a squeezed droplet is the only solution. However when the diameter is smaller than the height (Figure 4-b and c), two possi-

bilities may occur: either the droplet assumes a spherical shape or a "barrel" shape. This second case will happen if there is wetting of the channel floor and ceiling by the dispersed phase. We have recorded the frequency of the
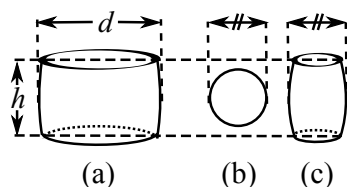

Figure 4: Sketch of droplet shape for (a) $d > h$ and (b) and (c) $d < h$.

droplet generation and compared it to theoretical estimations $f = Q_d/V$ where V is the droplet volume. We used two hypotheses for the droplet volume $V_s = \frac{1}{6}\pi d^3$ (spherical droplet) or $V_b \approx \frac{1}{4}\pi d^2 h$ (barrel/cylindrical droplet) when $d < h$. We see in Table 1 that in our experiments a barrel/cylindrical shape is present, even if this shape seems not at first thermodynamically favorable. This can be best explained if we assume that in our experiment the dispersed phase (oil) is wetting the floor and ceiling of the channels. We have independently verified with a manual contact angle measurement system from Nachet that the silicone oil does indeed wet the silicon and the glass used in the fabrication relatively well (contact angle, respectively, 21°and 31°). Actually if DI water wets silicon better (contact angle 14°) it does wet glass significantly less (contact angle 60°) supporting the hypothesis of a barrel shape for the droplet, which had already been suggested for describing the apparition of the balloon regime of droplet generation in our previous paper [9]. Still, we note that the measured contact angle is different from the contact angle in the chip as the surface energy there would have been modified by the bonding process. Wetting of the main channel silicon walls by oil has not been observed in normal operation, however we suspect that oil ends up on the walls, probably remaining in the fine grooves appearing there during the fabrication process ("scalloping" during the DRIE step visible in the inset in Figure 2), finally preventing the generation of droplets at the T-junction.

3   Model of droplet generation

For our experiments we have noticed that in the dripping regime the dependence of the droplet diameter with the dispersed phase velocity and dispersed channel width was not correctly described by existing analytical models from the literature [4, 10, 18]. In order to explain this difference, we reconsidered the formation mechanism of oil droplets in our microfluidic devices, where the dispersed

Experimental condition	Q_d (µL/min)	0,414	0,648	1,296
	Q_c (µL/min)	150	40	200
	w_d(µm)	10	10	20
	w_c(µm)	100	100	100
	h(µm)	46	72	72
Experimental result	d (µm)	35	68	58
	f(droplets/s)	154	40	110
Spherical model	f (droplets/s)	307	66	210
	error (%)	99,3	65	90,9
Barrel model	f (droplets/s)	156	41	114
	error (%)	1,3	2,4	3,5

Table 1: Comparison between experimental and theoretical droplet generation frequency using spherical and barrel model for the droplets shape ($d < h$).

phase is wetting the channel floor and ceiling. The exact dynamics of the droplet formation is complicated, and requires computer intensive numerical simulation, but we can express it in a qualitative way using analytical expression that captures most of the features of the process. Actually, from the sequence in Figure 5, we split the generation process in three main stages.

- Stage I: Arrival of the dispersed phase in the T-junction
  The droplet formation process starts when the oil reaches the T-junction at $t = t_0$. Then the oil enters the continuous phase micro-channel, and starts forming a cylindrical shape as it wets the floor and ceiling of the channel. Actually, this circular shape was also observed by Van der Graaf [16] at the beginning of the formation process of the oil in water droplet but they did not consider it as a separate stage. Moreover, it is almost absent of the formation process when we consider water-in-oil droplet (different wetting behavior), probably explaining why it had not been identified earlier. The inherent geometric stability of the circular shape compounded with the large interfacial tension and the low shear force exerted by the continuous phase (low viscosity of water) ensure that the cylindrical drop grows steadily. This stage ends when the drag force starts to deform the droplet at $t = t_I$ and the droplet starts leaning downstream towards the continuous phase micro-channel wall, without wetting it. At that time, the size of the droplet formed is only related to the width of the dispersed phase micro-channel w_d. Actually, the droplet has a circular shape, and forms an angle θ with the walls of the continuous phase micro-channel, as shown in Figure 6. This angle is constant and depends on the interface properties, especially on the wetting properties of the aqueous phase, but is different from the static contact angle measured

previously. The radius r_I of the droplet formed can be expressed by the following equation:

$$\sin\theta = \frac{w_d}{2r_I} \qquad (3)$$

This stage may seems anecdotal at first, but we have shown that by using a very low dispersed phase velocity, it is possible to remain in this stage until the droplet detaches. This gives rise to a new droplet generation regime with very specific features that we have dubbed the "balloon regime" [9].
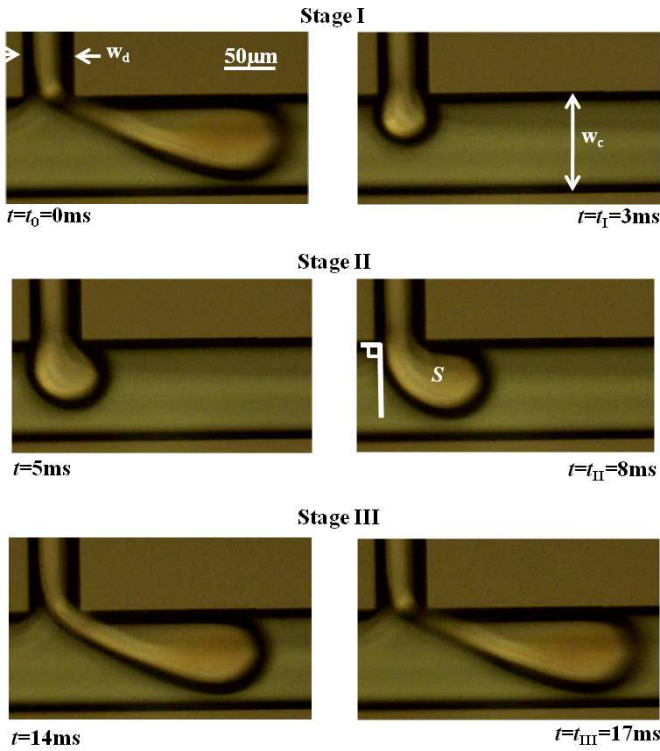

Stage I

$t=t_0=0$ms $t=t_1=3$ms

Stage II

$t=5$ms $t=t_{II}=8$ms

Stage III

$t=14$ms $t=t_{III}=17$ms

Figure 5: Mechanism of droplet formation with $w_c = 100$ µm, $w_d = 50$ µm, $h = 46$ µm, $\overline{v_d} = 1.5\,\mathrm{cm/s}$ and $\overline{v_c} = 7.25\,\mathrm{cm/s}$.

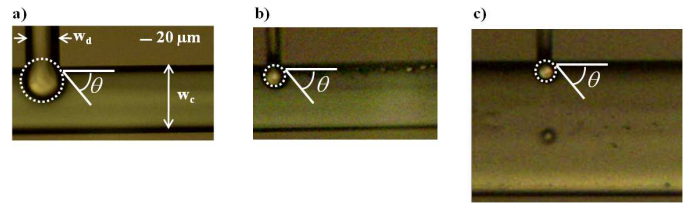

Figure 6: End of stage I in the mechanism of droplet formation, with $w_c = 100$ µm, $w_d = 50$ µm (a), $w_c = 100$ µm, $w_d = 20$ µm (b), $w_c = 200$ µm, $w_d = 20$ µm (c) and $h = 46$ µm, $\overline{v_d} = 1.5\,\mathrm{cm/s}$, $\overline{v_c} = 7.25\,\mathrm{cm/s}$. (Images are at the same scale.)

- Stage II: Swelling of the droplet
  During this stage, the droplet deforms and inflates before it starts to detach and, as suggested by previous authors [13, 16, 18], its shape is governed by an equilibrium between the forces arising from the interfacial tension and the drag.
  In our work, this stage ends at $t = t_{II}$ when the upstream side of the droplet is perpendicular to the wall of the continuous phase micro-channel, a time readily observed during our experiments (Figure 7). At this time, the droplet has deformed and its shape is roughly given by the sketch in Figure 8 where the surface of the droplet is S. We will now try to write
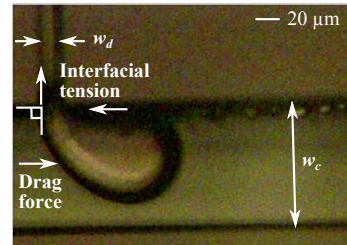

Figure 7: End of the stage II in the mechanism of droplet formation, with $w_c = 100$ µm, $w_d = 20$ µm and $h = 46$ µm.

in more detail the equilibrium of forces around the

oil droplet, along the continuous phase channel direction.

The interfacial tension gives rise to tension force that is tangent to the edges of the droplet at the wall of the continuous phase channel.
On the downstream part of the droplet, the force is directed along the continuous phase micro-channel wall and is given by:

$$F_{\text{tension}} = -h\sigma \quad (4)$$

the minus sign shows that it points in the upstream direction and tends to keep the droplet in place. At the upstream edge of the droplet, the force is perpendicular to the channel wall and has the same magnitude.
This is the same result as derived by Christopher [18] using Laplace's pressure argument, that is here directly implied by the definition used for the end of the equilibrium stage.

The drag force is composed of two components: a pressure component that can be expressed as $F_{\text{p}} = \Delta P A$, with ΔP the pressure difference on either side of the droplet, A the droplet cross-section area, and a shear component expressed by $F_{\text{s}} \propto \tau B = \mu_c \frac{\partial u}{\partial y} B$, with B the surface of the droplet parallel to the water flow and μ_c the dynamic viscosity of water.
The compact shape of the droplet at this instant of time ensures that the drag force is dominated by the pressure force instead of the shear force, which is aggravated in the case of oil-in-water droplet formation by the low value of the viscosity of the continuous phase liquid (μ_c of water). We thus write: $F_{\text{drag}} \approx F_{\text{p}} = \Delta P A \approx \Delta P h r$ where h is the micro-channel depth and r the micro-droplet radius.
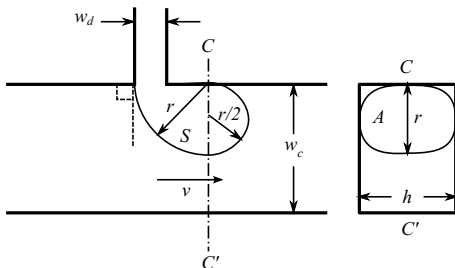

Figure 8: Idealized top and cross-section view of the droplet at $t = t_{\text{II}}$.

The expression we use to express the pressure drop ΔP is based on Poiseuille's pressure drop (equation 5) where the velocity that needs to be considered, as already suggested by Thorsen et al. [4], is the velocity in the gap between the droplet and the channel wall

$v = \frac{w_c}{w_c - r}\overline{v_c}$ where $\overline{v_c} = Q_c/hw_c$ is the average velocity of the continuous phase.

$$\Delta P = 32\frac{\mu_c w_c \overline{v_c} L (h + w_c - \epsilon)^2}{4h^2(w_c - \epsilon)^3} \quad (5)$$

This result is different from the lubrication or the simplified analysis done in the classical models [10, 18] that have been often reused in other studies. Using our notation, the pressure drop in the model of Garstecki et al. [10], can be written as:

$$\Delta P \approx 32\frac{\mu_c w_c \overline{v_c} L}{h(w_c - \epsilon)^2} \quad (6)$$

while in the model of Christopher et al. [18], it is:

$$\Delta P \approx 32\frac{\mu_c w_c \overline{v_c} L}{(w_c - \epsilon)^3} \quad (7)$$

We have been using the COMSOL MULTIPHYSICS software to compare the models of pressure drop. We used a squarish obstruction of varying thickness ϵ for representing the swelling droplet, and used an automatic meshing (fine) as the geometry was changing during the parametric study (before running the parametric study we verified for a few values of ϵ that a finer mesh gave results within 1% of the presented values). The increasing obstruction thickness resulted in an increase of the pressure drop ΔP as we see in Figure 9. The comparison between the simu-
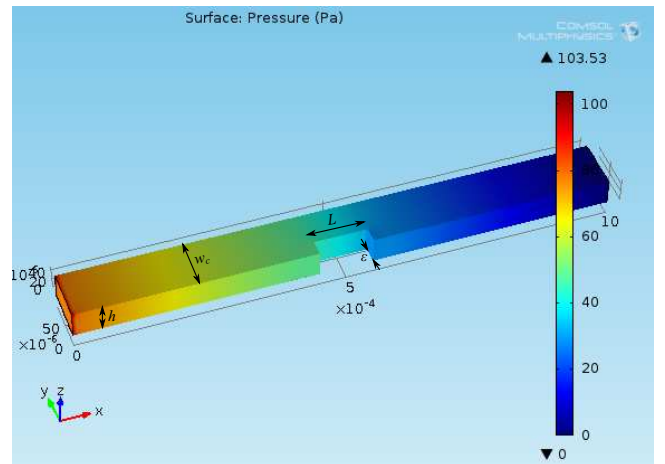

Figure 9: Pressure drop in the gap between the droplet and the wall of the continuous phase channel, with $h = 50$ µm, $w_c = 100$ µm, $\mu_c = 10^{-3}$ Pa.s, fluid velocity $\overline{v_c} = 1$ cm/s, $L = 100$ µm for $\epsilon = 30$ µm.

lated pressure drop for ϵ varying between 2µm and 98µm and the pressure drop used in our model and the models of Garstecki et al. [10] and Christopher
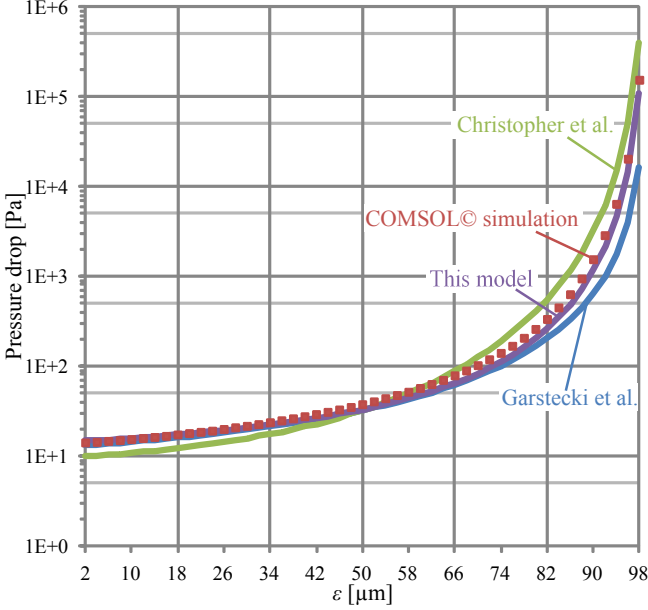
7

Figure 10: Comparison between the simulated pressure drop (dots) and the pressure drop used in our model and the models of Garstecki et al. [10] and Christopher et al. [18] (parameters are the same as in Figure 9).

et al. [18], is illustrated in Figure 10. We see that the expression used in our analytical model best approximates the simulated pressure drop (ΔP) in the system. Still we may note that when the channel is almost closed $(\epsilon > 0.9w)$, the square obstruction used in the simulation is blocking the flow much more than a real droplet will do, as the real rounded droplet won't fill the complete squarish section of the channel. In this range the simulation is probably overestimating the pressure drop by an increasingly large amount.

Thus, using simple geometric approximation $(A = hr)$ for the droplet cross-section area (Figure 8), we write:

$$F_{\text{drag}} \approx F_{\text{p}} \approx \frac{8\mu_c \overline{v}_c w_c r^2 (h + w_c - r)^2}{h(w_c - r)^3}$$

Finally, the equilibrium between the drag force and the interfacial tension gives:

$$F_{\text{tension}} + F_{\text{drag}} = -h\sigma + \frac{8\mu_c \overline{v}_c w_c r^2 (h + w_c - r)^2}{h(w_c - r)^3} = 0$$

This fourth order equation has two imaginary roots and two real roots with only one giving meaningful results for r. From simple geometric considerations on the droplet shape (Figure 8), we relate r to the droplet surface S and thus at the end of stage II, we

have:

$$S = \frac{3\pi}{8}r^2 \qquad (8)$$

- Stage III: Droplet detachment
  After $t = t_{\text{II}}$, the continuous phase starts detaching the droplet from the upstream edge of the dispersed phase micro-channel finally closing the oil flow into the droplet. The direction of droplet detachment is determined by the direction of water flow. The surface increase of the droplet s during this phase is related to the dispersed phase flow and can be expressed by:

$$s = t_{\text{neck}} \overline{v_d} w_d \qquad (9)$$

where $t_{\text{neck}} = t_{\text{III}} - t_{\text{II}}$ is the time it takes to shear the neck of the droplet originally of width r [19]. The time of necking is inversely proportional to the shear rate $(\mu_c \overline{v_c})$ imposed by the continuous phase, but it is also proportional to the viscosity of the dispersed phase, and thus the necking time is expressed in this work as $t_{\text{neck}} = \frac{r\mu_d}{\mu_c \overline{v_c}}$. We note that the viscosity ratio $\left(\frac{\mu_d}{\mu_c}\right)$ appearing here is absent from the earlier models in the literature [11, 12, 18, 19]. Moreover, in the case of water-in-oil droplet the viscosity ratio becomes very small, effectively making this phase very short and the surface increase s negligible. In that case the model would simplify and effectively stops at the end of stage II, as in the model of Thorsen [4] or Garstecki [10]. At the end of this stage at $t = t_{\text{III}}$, the droplet with a surface of $S + s$ is detached and a new cycle of droplet generation starts.

As the droplet reaches the storage chamber at the exit, it tends to assume a quasi cylindrical shape with height h and the diameter d of the drop is then given by:

$$d = \frac{1}{\sqrt{\pi}}\sqrt{S + s} \qquad (10)$$

The coefficient in front of $\sqrt{S + s}$ has been scaled by 0.5 by fitting the experimental results obtained for all our T-junction devices. Other types of junction would probably need another value for this factor, that take into account the intrinsic scaling approximation in the theory used to develop our model. Note that, according to our previous remarks, we did not introduce the capillary numbers $(Ca_c$ and $Ca_d)$ or flow rate (Q) in the model, but only kept $\overline{v_d}$, $\overline{v_c}$ and the channels dimensions.

4 Effect of the dispersed phase

During the experiment we observed that for the same velocity of the continuous phase, the micro-droplet size decreased when the width of the dispersed phase micro-channel w_d decreased (Figure 11).
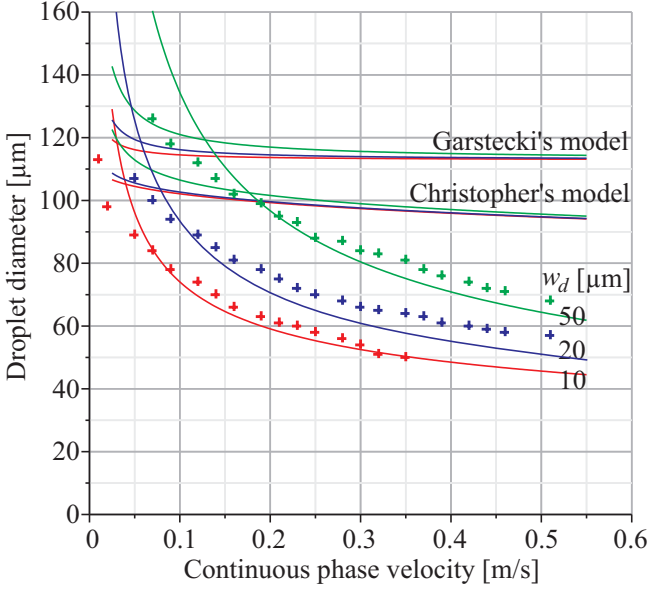
8

Figure 11: Effect of the width of the dispersed phase micro-channel on the diameter of the micro-droplet generated with $w_c = 100$ µm, $\overline{v_d} = 3$ cm/s, $h = 72$ µm and for w_d=10 µm, 20 µm, 50 µm. The cross indicates experimental points, while the line represent our model and the models from the literature ([18, 10]).

Figure 12: Effect of the velocity of the dispersed phase on the diameter of the micro-droplet generated with $w_c = 100$ µm, w_d=20 µm, $h = 72$ µm and for $\overline{v_d} = 0.75$ cm/s, 1.5 cm/s, 3 cm/s. The cross indicates experimental points, while the line represent our model and the models from the literature ([18, 10]).

At the end of the stage II, the surface S of the droplet is mostly governed by the velocity of the continuous phase $\overline{v_c}$, and the width of the continuous phase micro-channel w_c, but independent of the dispersed phase micro-channel geometry.

Actually, when the width of the continuous phase micro-channel is fixed ($w_c = 100$ µm) for a constant continuous phase $\overline{v_c}$, the section S of the droplet at $t = t_{II}$ is constant and mostly independent of w_d. Thus the volume of the droplet $V_{crit} = Sh$ is constant, and it can also be expressed by: $V_{crit} = Q_d t_{II}$, with Q_d the dispersed phase flow rate. As, $Q_d t_{II} = Sh$, then $w_d \overline{v_d} t_{II} = S =$ constant. The time required for swelling of the droplet depends on the micro-channel width and the velocity of the dispersed phase.

At stage III, as we clarified before, the droplet swelling is given by: $s = t_{neck} \overline{v_d} w_d$ with $t_{neck} = \frac{r\mu_d}{\mu_c \overline{v_c}}$. As S is constant, r is constant and t_{neck} is constant. By reducing the width of the dispersed phase micro-channel w_d at a constant velocity of the dispersed phase $\overline{v_c}$, the swelling of the droplet s during phase III is smaller, and the generated oil droplet is smaller.

Similarly, we observed that the droplet diameter decreased when the velocity $\overline{v_d}$ of the dispersed phase decreased (Figure 12).

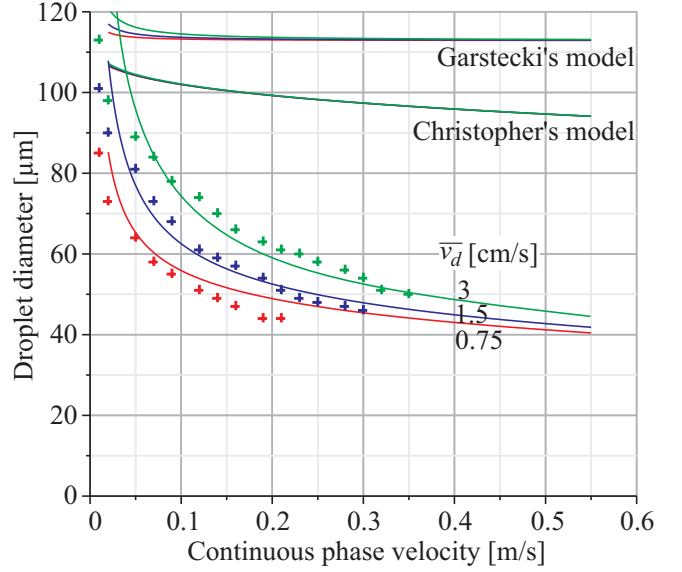As explained before, at the end of the stage II, the surface S of the droplet is mostly governed by the velocity of the continuous phase $\overline{v_c}$, and the width of the continuous phase micro-channel w_c, but independent of the dispersed phase velocity.

However, at stage III, the droplet swelling is given by: $s = t_{neck} \overline{v_d} w_d$ with $t_{neck} = \frac{r\mu_d}{\mu_c \overline{v_c}}$. As S is constant, r is constant and t_{neck} is constant. By reducing the velocity of the dispersed phase $\overline{v_d}$ at a constant width of the dispersed phase micro-channel w_c, the swelling of the droplet s during phase III is smaller, and the generated oil droplet is smaller.

We note that if the dispersed phase velocity is sufficiently reduced (here if $\overline{v_d} < 0.6$cm/s), the regime of droplet generation changes. Actually, it goes from the dripping regime to the balloon regime [9], which is not described by the model discussed in this paper.

We also noticed that the behavior was almost insensitive to the depth of the micro-channels h (Figure 13). This relative insensitivity exists also in the model when $h \gg w_c - r$ in the numerator of F_{drag}, that is when $w_c \approx r$ – which is generally the practical case that has actually been considered previously in some models ([10]). In this simpler case we can verify that the term h can be completely removed from the model.

In Figure 11 and Figure 12 we plotted the prediction from two different models from the literature [10, 18] and of our model against the experimental results. The analytical models available in the literature [4, 16, 10, 18] failed to predict the observed dependency with w_d or v_d. Even if
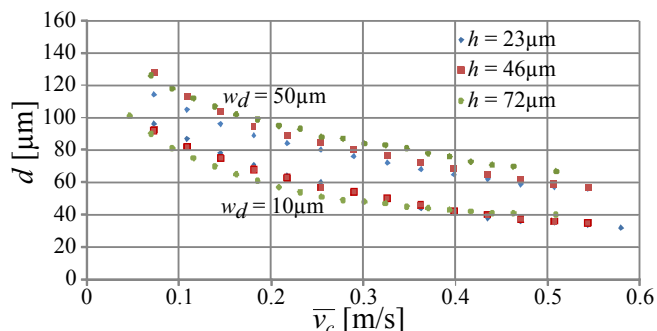
Figure 13: Effect of the depth of the dispersed phase micro-channel on the diameter of the micro-droplet generated with $\overline{v_d} = 1.5$ cm/s, $w_c = 100$ µm and (circle) $h = 72$ µm, (square) $h = 46$ µm, (diamond) $h = 23$ µm.

the literature models could be adjusted (scaling) to match the amplitude of the experimental value more closely, it is clear that the power law dependence as a function of $\overline{v_c}$ is substantially different from what we observe experimentally. Apparently, this difference stems in part from an increased duration of the third phase of the swelling, as the viscosity effects are important in our configuration where oil (and not water) droplets are generated. Moreover, as we clarified before, our set-up generates "cylindrical" droplets in the dripping regime, which may not be the case in all the literature experiments. We clearly see that in this case the observed experimental behavior is much better described by our model.

Still we note in our model that larger error appears with larger droplets. Actually, when the droplet diameter approaches the width of the continuous phase micro-channel ($w_c =100$ µm in Figure 11 and Figure 12), the generation regime changes and goes toward the squeezing regime, which is not described by our model, but is better described by Garstecki's model [10].

5 Effect of the continuous phase

We observed experimentally that at the same velocity of the continuous phase, the micro-droplet size decreased when the width w_c of the continuous phase micro-channel decreased (Figures 14) but was again, for the same reason as before, very weakly dependent on the depth h of the micro-channel.

Actually, during stage II, as we clarified before, S is a function of w_c and $\overline{v_c}$, when the width of the continuous phase micro-channel w_c decreases at constant flow velocity $\overline{v_c}$, the droplet surface S reached at the end of phase II decreases (Figure 15).

At stage III, t_{neck} decreases since it is a function of r. As w_d and v_d are constants, the swelling s of the droplet at $t = t_{III}$ decreases.
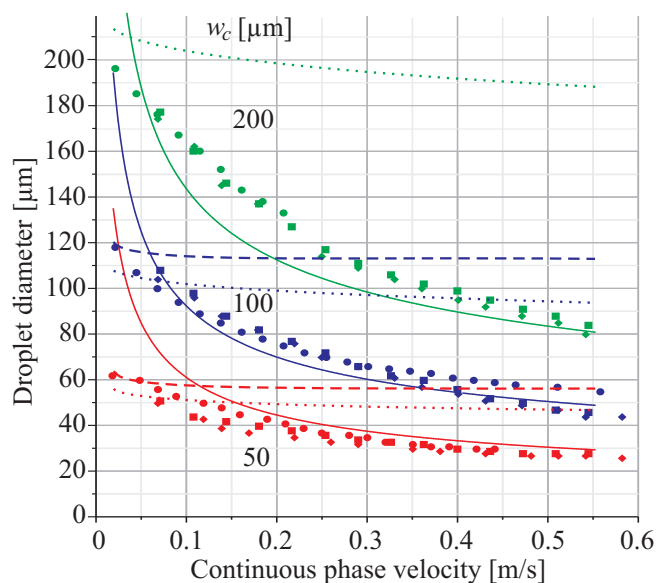

Figure 14: Effect of the width and the depth of the continuous phase micro-channel on the diameter of the micro-droplet generated with $w_d = 20$ µm, $\overline{v_d} = 1.5$ cm/s. Experimental points for (circle) $h = 72$ µm, (square) $h = 46$ µm, and (diamond) $h = 23$ µm. Model simulation with (full line) this model, (dashed line) Garstecki's model [10], and (dotted line) Christopher's model [18].

Thus the final surface of the droplet $(S + s)$ decreases, and the final diameter of the generated droplet becomes smaller.

The observed behavior is again similar to what is predicted by our model (Figure 14) and the comparison with the classical models shows again that our experiments are different from previous work. We still note that for bigger droplets (lower $\overline{v_c}$) the difference with our model starts to be significant. Actually, here again, when the droplet diameter (d) reaches the value of the continuous micro-channel width (w_c), we tend to leave the dripping regime and reach the squeezing regime, where our model is no more valid but which is adequately described by Garstecki's model [10] for example.

As already reported in different publications [14, 26, 27], the micro-droplet diameter also decreased when the velocity of the continuous phase $\overline{v_c}$ increased in the same microfluidic configuration (w_d and w_c are fixed). Actually, during stage II, the tension force that holds the droplet is constant because it is proportional to the interfacial tension and the micro-channel depth that are kept constant. Thus, the force required to detach the droplet remains constant. Accordingly, as the velocity of the continuous phase increases, the drop cross-section and r decreases, and the droplet surface S decreases.
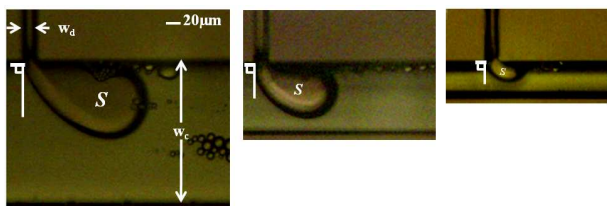
Figure 15: Effect of the width of the continuous phase micro-channel on the droplet section at the end of stage II with $w_d = 20$ µm, $h = 46$ µm, $\overline{v_d} = 1.5$ cm/s, $\overline{v_c} = 7.25$ cm/s, and $w_c = 200$ µm (a), $w_c = 100$ µm (b), $w_c = 50$ µm (c). (Images are at the same scale.)

6 Conclusion

In the present work, monodisperse oil droplets in water were generated using a T-junction configuration. Microfluidic devices made on silicon-glass were fabricated with different cross-sections of the continuous and dispersed phases micro-channels to study the effect of the micro-channels geometry on the micro-droplet size.

We showed that the dripping regime can be obtained at very low capillary number by using deionized water as the continuous phase and a silicone oil with a large interfacial tension as the dispersed phase.

We found that the dependence of the droplet diameter with geometry and velocity did not coincide with existing analytical models. In order to explain this behavior, we divided the mechanism of micro-droplet formation into three stages where we considered wetting of the dispersed phase at the floor and ceiling of the microchannel. During stage I, the droplet has a circular shape. When the droplet deforms, stage II starts and the droplet grows. We define the end of this stage when the droplet is tangent to the upstream edge of the dispersed phase microchannel. Finally, stage III corresponds to the phase seeing the detachment of the micro-droplet. We then proposed an analytical model of the dripping regime for oil-in-water microdroplet generation. The model could predict the observed behavior better than existing models, highlighting a difference in our setup presumably linked with the dispersed phase wetting of the main channel floor and ceiling. Nonetheless, it is clear that some finer behavior of this process are still incompletely described and will require more investigation in the future, particularly to extend the scaling laws to smaller droplet diameters.

Acknowledgments

References

[1] George M. Whitesides. The origins and the future of microfluidics. *Nature*, 442:368–373, 2006.

[2] Gi Hun Seong, Wei Zhan, and Richard M. Crooks. Fabrication of microchambers defined by photopolymerized hydrogels and weirs within microfluidic systems: Application to DNA hybridization. *Anal. Chem.*, 74:3372–3377, 2002.

[3] N.T. Nguyen, S. Lassemono, F. Chollet, and Charles Yang Chun. Interfacial tension measurement with an optofluidic sensor. *IEEE Sensors*, 7:692–697, 2007.

[4] T. Thorsen, R. W. Roberts, F. H. Arnold, and S. R. Quake. Dynamic pattern formation in a vesicle-generating microfluidic device. *Physical Review Letters*, 86:4163–4166, April 2001.

[5] Alfonso M. Gañán-Calvo and José M. Gordillo. Perfectly monodisperse microbubbling by capillary flow focusing. *Phys. Rev. Lett.*, 87:274501, 2001.

[6] P. B. Umbanhowar, V. Prasad, and D. A. Weitz. Monodisperse emulsion generation via drop break off in a coflowing stream. *Langmuir*, 16:347–351, 2000.

[7] C. Cramer, P. Fischer, and E. J. Windhab. Drop formation in a co-flowing ambient fluid. *Chemical Engineering Science*, 59:3045–3058, 2004.

[8] I. Kobayashi, S. Mukataka, and M. Nakajima. Effects of type and physical properties of oil phase on oil in water emulsion droplet formation in straight through microchannel emulsification, experimental and CFD studies. *Langmuir*, 21:5722–5730, 2005.

[9] Nathalie Tarchichi, Franck Chollet, and Jean-François Manceau. New regime of droplet generation in a T-shape microfluidic junction. *Journal of Microfluidics and Nanofluidics*, 14:45–51, 2013.

[10] Piotr Garstecki, Michael J. Fuerstman, Howard A. Stone, and George M. Whitesides. Formation of droplets and bubbles in a microfluidic T-junction-scaling and mechanism of break-up. *Lab Chip*, 6(3):437–446, Mar 2006.

[11] J. Xu, S. Li, J. Tan, and G. Luo. Correlations of droplet formation in T-junction microfluidic devices: from squeezing to dripping. *Microfluidics and Nanofluidics*, 5:711–717, 2008.

[12] Taotao Fu, Youguang Ma, Denis Funfschilling, Chunying Zhu, and Huai Z. Li. Squeezing to dripping transition for bubble formation in a microfluidic T-junction. *Chemical Engineering Science*, 65:3739–3748, 2010.

[13] G. I. Taylor. The formation of emulsions in definable fields of flow. *Proceedings of the Royal Society of London. Series A, Containing Papers of a Mathematical and Physical Character*, 146(858):pp. 501–523, 1934.

[14] T. Nisisako, T. Torii, and T. Higuchi. Droplet formation in a microchannel network. *Lab on a chip*, 2:24–26, 2002.

[15] V. Cristini and YC Tan. Theory and numerical simulation of droplet dynamics in complex flows–a review. *Lab Chip*, 4:257–264, 2004.

[16] S. van der Graaf, M.L.J. Steegmans, R.G.M. van der Sman, C.G.P.H. Schroen, and R.M. Boom. Droplet formation in a T-shaped microchannel junction: A model system for membrane emulsification. *Colloids and Surfaces A: Physicochemical and Engineering Aspects*, 266:106–116, 2005.

[17] S.J. Peng and R.A. Williams. Controlled production of emulsions using a crossflow membrane: Part I: Droplet formation from a single pore. *Chemical Engineering Research and Design*, 76(8):894–901, 1998.

[18] G. F. Christopher, N. N. Noharuddin, J. A. Taylor, and S. L. Anna. Experimental observations of the squeezing-to-dripping transition in T-shaped microfluidic junctions. *Phys. Rev. E*, 78(3):036317, September 2008.

[19] Sujin Yeom and Sang Yong Lee. Dependence of micro-drop generation performance on dispenser geometry. *Experimental Thermal and Fluid Science*, 35:1565–1574, 2011.

[20] M. De Menech, P. Garstecki, F. Jousse, and H. A. Stone. Transition from squeezing to dripping in a microfluidic T–shaped junction. *journal of fluid mechanics*, 595:141–161, 2008.

[21] Jayaprakash Sivasamy, Teck-Neng Wong, Nam-Trung Nguyen, and Linus Tzu-Hsiang Kao. An investigation on the mechanism of droplet formation in a microfluidic T junction. *Microfluid Nanofluid*, 11:1–10, 2011.

[22] N. Tarchichi, F. Chollet, and J. F. Manceau. Dispersed phase velocity controlled regime of microdroplets generation in T-junction. In *Micro FLU12-13, Heidelberg*, 2012.

[23] J. Cooper Mcdonald and George M. Whitesides. Poly(dimethylsiloxane) as a material for fabricating microfluidic devices. *Accounts of chemical research*, 35:491–499, 2002.

[24] Taotao Fu, Youguang Ma, Denis Funfschilling, and Huai Z. Li. Bubble formation and breakup mechanism in a microfluidic flow-focusing device. *Chemical Engineering Science*, 64:2392–2400, 2009.

[25] K. Dopierala, A. Javadi, J. Krägel, K.-H. Schano, E.P. Kalogiannid, M.E. Leser, and R. Miller. Dynamic interfacial tensions of dietary oils. *Colloids and Surfaces A*, 382:261–265, 2011.

[26] Yung-Chieh Tan, Vittorio Cristini, and Abraham P. Lee. Monodispersed microfluidic droplet generation by shear focusing microfluidic device. *Sensors and Actuators B*, 114:350–356, 2006.

[27] J. Tan, S.W. Li, K. Wang, and G.S. Luo. Gas liquid flow in T-junction microfluidic devices with a new perpendicular rupturing flow route. *Chemical Engineering Journal*, 146:428–433, 2009.